Uncertainties in multi-temperature nonequilibrium partition functions and application to CO2

Ulysse Dubuet, E. Pannier, C.O. Laux

▶ **To cite this version:**

Ulysse Dubuet, E. Pannier, C.O. Laux. Uncertainties in multi-temperature nonequilibrium partition functions and application to CO2. Journal of Quantitative Spectroscopy and Radiative Transfer, 2022, 290, pp.108314. 10.1016/j.jqsrt.2022.108314 . hal-04441750

HAL Id: hal-04441750
https://hal.science/hal-04441750

Submitted on 2 May 2024

HAL is a multi-disciplinary open access archive for the deposit and dissemination of scientific research documents, whether they are published or not. The documents may come from teaching and research institutions in France or abroad, or from public or private research centers.

L'archive ouverte pluridisciplinaire **HAL**, est destinée au dépôt et à la diffusion de documents scientifiques de niveau recherche, publiés ou non, émanant des établissements d'enseignement et de recherche français ou étrangers, des laboratoires publics ou privés.

Uncertainties in Multi-Temperature Nonequilibrium Partition Functions and Application to CO_2

U. Dubuet, E. Pannier, C. O. Laux
Laboratoire EM2C, CNRS UPR288, CentraleSupélec, Université Paris-Saclay, 3 rue Joliot-Curie, 91190 Gif-sur-Yvette, France

Keywords: nonequilibrium partition functions, interaction and coupling terms in CO2, multi-temperature models, energy mode grouping

Abstract

Multi-temperature models are often used as a simplified way to describe nonequilibrium gases. These models assume Boltzmann distributions within each energy mode, which is useful for reducing the number of parameters in computations. This assumption requires that the energy modes are properly separated (which is valid, for instance, for vibration and rotation in low-lying rovibrational levels of diatomic molecules). For polyatomic molecules, several limitations arise. First, certain energy modes are often grouped together to further reduce the number of parameters, which requires additional hypotheses, and sometimes arbitrary grouping schemes. Moreover, the rovibrational levels of polyatomic molecules are often strongly coupled, and the assignment of the coupling terms to one or another energy mode is arbitrary. In this work, we present a method to quantify the influence of assignment or grouping schemes on nonequilibrium spectral models by comparing their impact on nonequilibrium partition functions, and we apply it to the CO_2 molecule. We show that significant differences arise when reducing the nonequilibrium model to two temperatures only, as often done in CFD or spectroscopy applications. In particular, one should carefully justify whether the vibrational bending mode is in equilibrium with the rotational mode or with the other vibrational modes. We then determine the nonequilibrium range where a simple Uncoupled Vibrating Rotor model is sufficient, where the coupling term assignment scheme becomes important, and where the uncertainty induced by the assignment of the coupling terms can no longer be neglected. This approach can be extended to other molecules.

1 Introduction

Numerical simulations of molecular spectra require determining the population of the internal energy levels of the molecule. Under nonequilibrium conditions, the most accurate way to describe them is to use level-specific models, where the population of each level is calculated from the kinetic equations resulting from the interaction with other levels. However, these models, such as [1]–[5], are often computationally too expensive for applications such as computational fluid dynamic calculations (CFD), spectral fitting, or kinetic models of nonequilibrium gases. To reduce the cost of the computations, it is often assumed that these populations follow specific distributions (e.g., Boltzmann or Treanor) at characteristic temperatures that may differ depending on the internal energy modes (e.g., T_{rot}, T_{vib} for rovibrational levels of diatomic molecules) [6–10]. The use of multi-temperature models (T_{vib}, T_{rot}, etc.) is valid as long as the exchange rates within an energy mode are much higher than the exchange rates between different energy modes. For polyatomic molecules, however, the rovibrational levels can be coupled by strong interaction terms, and the separation of the energy terms is not as straightforward as for diatomic molecules.

Furthermore, high-performance calculations often require limiting the number of parameters, which then requires grouping the energy modes (e.g., define only one vibrational temperature for all vibrational modes of a polyatomic molecule). Different grouping schemes are then possible and should be compared.

This paper proposes to assess the uncertainties induced by the reduction of degrees of freedom in nonequilibrium spectral models in order to derive a domain of validity for multi-temperature models.

Section 2 presents a simple model, the Uncoupled Vibrating Rotor (UVR) model, to obtain the energy of CO_2 rovibrational levels. This model will serve for baseline comparisons with more detailed models. In Section 3, we present how to assess the uncertainties introduced when grouping energy modes in two-temperature models and we apply the method to the CO_2 molecule for two common temperature groupings. We proceed analogously to Babou *et al.* [11] by comparing extreme cases using the differences in the partition functions. In Section 4, we present a method to assess the impact of coupling terms on polyatomic molecule partition functions and a general method to separate the rotational, vibrational and coupling energy terms using the molecule's Hamiltonian. We apply these methods to the CO_2 molecule in Section 5: first, we compute the different energy terms and compare them to the coupling terms, and then evaluate the impact of the latter on CO_2 partition functions using the two-temperature models compared in Section 3. We obtain domains where the simpler UVR model is sufficient to accurately describe the CO_2 molecule and domains where the coupling terms should be considered. The impact of the various assignment and coupling schemes is illustrated in practical examples in Section 6.

2 The Uncoupled Vibrating Rotor model

To compare multi-temperature models, we use the rovibrational partition function. To simplify, at first, we neglect the coupling terms, thus assuming that the various energy modes are uncoupled. For the CO_2 molecule, for instance, we obtain the following nonequilibrium partition function for a four-temperature Boltzmann distribution at the temperatures T_{vib1}, T_{vib2}, T_{vib3} and T_{rot}:

$$Q_{rovib}(T_{vib}, T_{rot}) = \sum_{v} \left[g_{vib1} e^{-\frac{E_{vib1}(v)}{kT_{vib1}}} g_{vib2} e^{-\frac{E_{vib2}(v)}{kT_{vib2}}} g_{vib3} e^{-\frac{E_{vib3}(v)}{kT_{vib3}}} \left(\sum_{J} g_{rot}(J) e^{-\frac{E_{rot}(v,J)}{kT_{rot}}} \right) \right] \quad (2.1)$$

with g the degeneracy and k the Boltzmann constant. Note that such multi-temperature Boltzmann distributions may not be valid under all conditions. In that case, state-to-state population modeling, such as in Ref. [12], is required.

The vibrational (symmetric stretching, bending and asymmetric stretching) energies and rotational energy can be calculated with the Uncoupled Vibrating Rotor (UVR) model, which is based on the Dunham expansion.

For the CO_2 molecule, the UVR model features a first-order correction of the anharmonicity for the three vibrational modes ($w_e x_{e1}$, $w_e x_{e2}$, $w_e x_{e3}$ in Eq. (2.2)) and a second-order correction of the centrifugal force (D_e and H_e in Eq. (2.3)). It does not, however, consider the vibrational-rotational couplings or the different interactions between CO_2 rovibrational levels (such as the Fermi interaction).

$$E_{vib,i} = \omega_{e,i} \left(v_i + \frac{g_i}{2} \right) - \omega_e x_{e,i} \left(v_i + \frac{g_i}{2} \right)^2, i = 1,2,3 \quad (2.2)$$

$$E_{rot} = B_e \left[J(J+1) - l_2^2 \right] - D_e \left[J(J+1) - l_2^2 \right]^2 + H_e \left[J(J+1) - l_2^2 \right]^3 \quad (2.3)$$

In the present work, the energies E_{vib1}, E_{vib2}, E_{vib3}, E_{rot} of the UVR model are calculated with the spectroscopic constants reviewed in Ref. [7].

However, for a two-temperature Boltzmann distribution at T_{vib} and T_{rot}, the rovibrational partition function is calculated as follows:

$$Q_{rovib}(T_{vib}, T_{rot}) = \sum_{v} \left[g_v e^{-\frac{\bar{E}_{vib}(v)}{kT_{vib}}} \left(\sum_{J} g_{rot}(J) e^{-\frac{\bar{E}_{rot}(v,J)}{kT_{rot}}} \right) \right] \quad (2.4)$$

To reduce the 4 energy terms into one vibrational energy $\bar{E}_{vib}$ and one rotational energy $\bar{E}_{rot}$, assumptions must be made on the grouping of the energy modes (i.e., define a temperature grouping scheme). For example, one can choose $\bar{E}_{vib} = E_{vib1} + E_{vib2} + E_{vib3}$ and $\bar{E}_{rot} = E_{rot}$.

We present the impact of these assumptions for a two-temperature model in the following Section.

3 Temperature grouping schemes and their impact for CO_2

To obtain simplified models, one can group levels that have approximately the same energy distribution. We define the temperature grouping scheme as the way we group the energy modes together.

For CO_2, levels that differ only by the value of their orbital momentum l_2 are usually grouped into a $g=v_2+1$ degenerate v_2 level. Similarly, the levels of a Fermi-interacting group that shares the same v_1+2v_2 number are often lumped. The description of the rovibrational levels is then reduced to a three-temperature model with T_{vib12}, T_{vib3} and T_{rot}, where $T_{vib12} = T_{vib1} = T_{vib2}$.

To further reduce the model to a two-temperature model requires assessing which of the vibrational-vibrational (VV) relaxation between the $\nu_{1,2}$ and ν_3 modes, or the vibrational-rotational (VR) relaxation between ν_{12} and J, is faster.

Different experimental conditions show different results and thus justify the need for different grouping schemes.

For example, the grouping scheme $T_{rot} = T_{vib1,2,rot}$ and $T_{vib} = T_{vib3}$ is often used to analyze discharge experiments, such as in Refs. [13], [14]. Indeed, studies of a continuous wave CO_2 laser discharge [13] showed $T_{vib1,2} \sim T_{rot} \ll T_{vib3}$ (typically: $T_{vib1,2}$, $T_{rot} < 500$ K, $T_{vib3} > 1500$ K) whereas studies of a low-pressure carbon monoxide flame [14] found $T_{12} \sim T_{rot} \gg T_3$ ($T_{12} = 2150$ K, $T_3 = 1040$ K at 76 torr). These two experiments show that $T_{vib1,2} \sim T_{rot} \neq T_{vib3}$. This assumption is also supported by recent calculations of vibrational energy exchange cross-sections in CO_2 – CO_2 collisions at $T_{rot} = 1000 – 3000$ K [15], which showed a large interaction between the ν_1 and ν_2 modes, but no energy transfer from the ν_2 to the ν_3 mode.

On the other hand, the grouping scheme $T_{vib} = T_{vib1,2,l_2,3}$, T_{rot} is commonly used [16], [17] to analyze shock and expansion-tube experiments [10], [18], [19]. To our knowledge, no experimental results support this temperature grouping, but the relatively does not allow a precise determination of the vibrational level distributions.

We can now quantify the impact of the chosen grouping scheme for the simple case where we neglect the coupling terms, i.e., where the energies E_{vib1}, E_{vib2}, E_{vib3}, E_{rot} are calculated using the uncoupled vibrating rotor (UVR) model described in Section 2. We calculate $^{12}C^{16}O_2$ nonequilibrium partition functions with a two-temperature model for the following temperature grouping schemes:

Scheme 1: $\{T_{vib}, T_{rot}\} = \{(T_{vib1}, T_{vib2}, T_{vib3}), (T_{rot})\}$

Scheme 2: $\{T_{vib}, T_{rot}\} = \{(T_{vib3}), (T_{vib1}, T_{vib2}, T_{rot})\}$

The partition functions are given by Eq. (3.1) for the first scheme and Eq. (3.2) for the second scheme.

$$Q_1(T_{vib}, T_{rot}) = \sum_{(v,J)} g_{v,J} \exp\left(-\frac{E_{vib1} + E_{vib2} + E_{vib3}}{kT_{vib}} - \frac{E_{rot}}{kT_{rot}}\right) \tag{3.1}$$

$$Q_2(T_{vib}, T_{rot}) = \sum_{(v,J)} g_{v,J} \exp\left(-\frac{E_{vib3}}{kT_{vib}} - \frac{E_{vib1} + E_{vib2} + E_{rot}}{kT_{rot}}\right) \tag{3.2}$$

Figure 1 carries the main message of this paper: it shows that the nonequilibrium partition functions calculated with the two grouping schemes can be very different.

CO_2 is highly sensitive to the choice of the temperature grouping scheme, in particular to the assignment of T_{vib2} in the distribution model, because the vibrational partition function of the ν_2 mode is much larger than the partition functions of the other modes owing to the numerous sublevels of different orbitals l_2.

We also represented in Figure 1 several experimental data points corresponding to measurements in expansion-tubes [10, 17, 18] (crosses), CO_2 lasers [13] (dot), CO_2 glow discharges [7] (squares), and CO_2 NRP discharges [20] (triangles). Many of these experimental conditions fall into regions with large differences between the nonequilibrium partition functions

calculated with the two different grouping schemes, and are thus very sensitive to the rotational and vibrational temperature groupings.

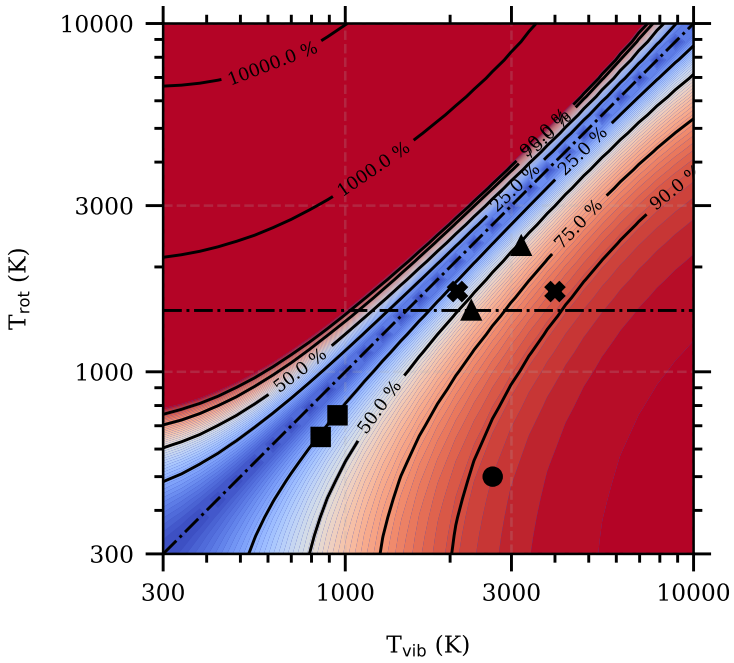

Figure 1 Relative differences between nonequilibrium partition functions of CO_2 for two-temperature Boltzmann distributions using the UVR model, with two grouping schemes: $\{T_{vib}, T_{rot}\} = \{(T_{vib1}, T_{vib2}, T_{vib3}), (T_{rot})\}$ and $\{T_{vib}, T_{rot}\} = \{(T_{vib3}), (T_{vib1}, T_{vib2}, T_{rot})\}$. The symbols correspond to experimental data points: expansion-tube [10, 17, 18] (crosses), CO_2 lasers [13] **(dot), CO_2 glow discharges [7] (squares) and CO_2 NRP discharges** [20] **(triangles).**

Figure 2 shows the relative difference between the nonequilibrium partition functions calculated with the two grouping schemes for a given rotational temperature of 1500 K (along the dash-dot line in Figure 1). We also show with a vertical dashed line the point of thermal equilibrium, i.e., where the vibrational temperature is equal to the rotational temperature. The partition functions are identical at this temperature but rapidly differ by up to 450% when the vibrational temperature is lower than the rotational one and by up to 100% in the opposite situation.

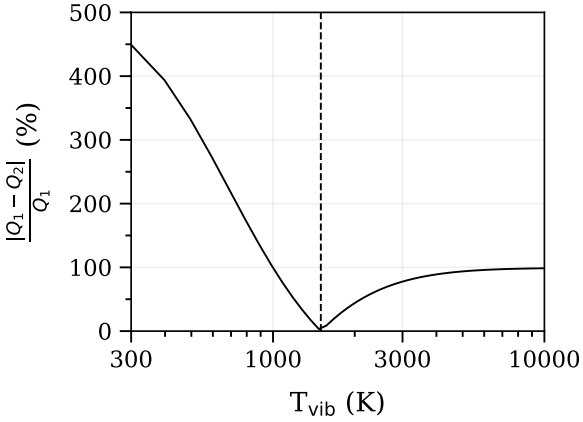

Figure 2 Relative differences between nonequilibrium partition functions of CO_2 for two-temperature Boltzmann distributions using the UVR model for a rotational temperature T_{rot}=1500 K. The vertical dashed line shows the equilibrium vibrational temperature (T_{vib}=1500 K).

To further illustrate the importance of the temperature grouping scheme on simulated spectra, we compare in Figure 3 the transmittance spectra calculated using the two temperature grouping

schemes, using the same conditions as Dang *et al.* [13] (circle in Figure 1). The simulations were performed using the UVR model for the computation of the partition functions and level populations and the CDSD-4000 database [21] for the line positions and line widths.

The two simulated spectra (black and red lines) exhibit major differences: while the black line, corresponding to Q_2 in Eq. (3.2), agrees well with the measurements of Dang *et al.* [13][1], the red line, using a different grouping scheme and corresponding to Q_1 in Eq. (3.1), does not fit the experimental data at all.

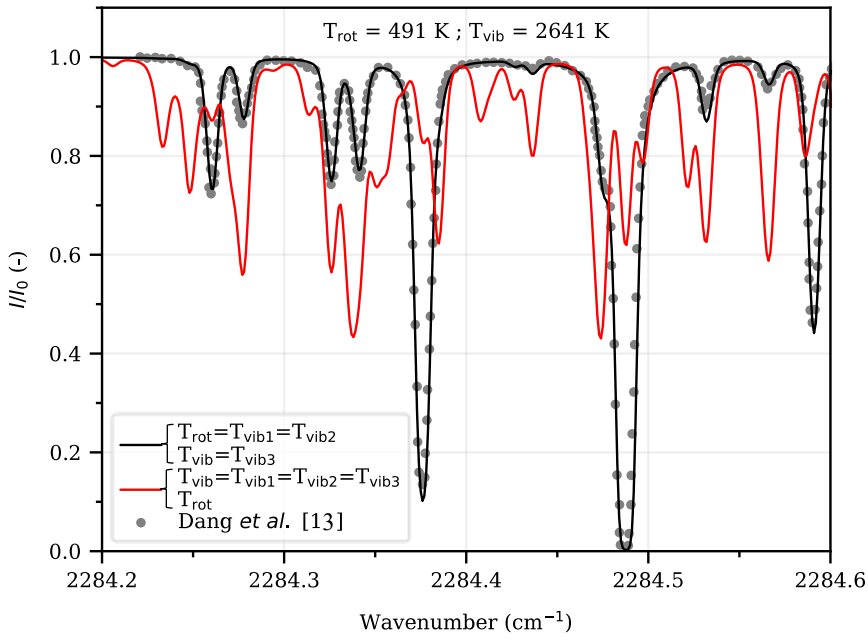

Figure 3 Comparison of transmittance using the two grouping schemes (black and red lines) under the CO2 laser [13] **experimental conditions (grey dots).**

The choice of the temperature grouping can thus induce large discrepancies in the simulated spectra, thus strongly affecting experimental analyses of spectroscopic data. This choice is not always reported in the literature. For instance, the NASA NEQAIR Line-By-Line code [9], [16] uses a CO_2 nonequilibrium model based on the CDSD database by defining the vibrational energy as the minimum energy of each polyad[2]. This grouping scheme is very close to the assumption that all three vibrational modes are in equilibrium, and thus that $T_{vib} = T_{vib1} = T_{vib2} = T_{vib3}$. This is a strong assumption, and it should be carefully considered based on the physical system being studied.

4 Impact of the coupling terms

[1] We used here a two-temperature model (T_{vib}=T_{vib3}=2641 K and T_{rot}=T_{vib1}=T_{vib2}=491 K) instead of a three-temperature model with small differences between the rotational temperature and the temperature of the first two vibrational modes (T_{rot}=491K, T_{vib1}=T_{vib2}=514 K and T_{vib3}=2641 K) as did Klarenaar *et al.* [7]. This does not induce significant discrepancies.

[2] For CO_2, the polyad p groups all vibrational levels such as $p = 2v_1 + v_2 + 3v_3$. For other molecules, the definition of the polyad can be obtained using [33].

4.1 Nonequilibrium partition functions with coupling terms in a two-temperature model

We now consider the more general case including the coupling energy terms. In a two-temperature model using Boltzmann distributions at T_{vib} and T_{rot}, the rovibrational partition function is usually calculated as follows:

$$Q_{rovib}(T_{vib}, T_{rot}) = \sum_{v} \left[g_v e^{-\frac{E_{vib}(v)}{kT_{vib}}} \left(\sum_{J} g_{rot}(J) e^{-\frac{E_{rot}(v,J)}{kT_{rot}}} \right) \right] \tag{4.1}$$

where E_{vib} and E_{rot} are the vibrational and rotational energies, and g_v, g_{rot} are the vibrational and rotational degeneracies, respectively.

The rovibrational energies can be written as the sum of the uncoupled energies of each energy mode ($\bar{E}_{vib}$, $\bar{E}_{rot}$) and of the coupling terms ($E_{coupling}$):

$$E(v, J) = \bar{E}_{vib}(v) + \bar{E}_{rot}(J) + E_{coupling}(v, J) \tag{4.2}$$

Vibrational-rotational coupling terms appear as diagonal terms in the Hamiltonian and produce the α_e and β_e terms in the usual Dunham expansions. The rotational energy E_{rot} usually includes the correction to the rigid rotor rotational energy, but this correction can also be assigned to the vibrational energy [22]. The choice derives from the construction of the Dunham development, which results from a polynomial expansion of the electronic potential energy $V(r)$, where r is the bond length. The rovibrational energy is expressed as:

$$E(v, J) = G(v) + F_v(J) \tag{4.3}$$

where G is the vibrational energy and F_v the rotational energy for a given vibrational level v. Hence the rotational-vibrational coupling terms, which depend on both the vibrational and rotational quanta v and J, are naturally assigned to $F_v(J)$.

Other models, such as the Liu & Vinokur model [23], use instead a polynomial expansion of the total potential energy $U_J(r) = V(r) + h^2/(8\pi^2\mu)\, J(J+1)/r^2$, which includes the rotational energy, with μ the reduced mass of the molecule and r the interatomic distance. In such a model, the rovibrational energy is expressed as:

$$E(v, J) = F(J) + G_J(v) \tag{4.4}$$

where F is the rotational energy and G_J is the vibrational energy for a given rotational level J. In the Liu & Vinokur model (Appendix A of Ref. [22]), the vibrational-rotational coupling terms are naturally included in the vibrational energy term G_J.

The other coupling terms do not appear explicitly in Dunham expansions and are non-diagonal in the molecule's Hamiltonian. For CO_2, the levels are affected by the Fermi interaction (or Fermi resonance) (e.g., between levels (1,0,0) and (0,2,0) with the (v_1,v_2,v_3) notation for CO_2), by the l-doubling interaction (between two levels whose l_2 quantum numbers slightly differ ($\Delta l_2 = \pm 2$)), and by the Coriolis interaction.

The coupling terms are far smaller than the sum of the vibrational and rotational terms ($E_{coupling} \ll \bar{E}_{vib} + \bar{E}_{rot}$). Hence, under equilibrium conditions ($T_{vib} = T_{rot}$), they have little impact on the partition functions:

$$\frac{\bar{E}_{vib} + \bar{E}_{rot} + E_{coupling}}{T} \approx \frac{\bar{E}_{vib} + \bar{E}_{rot}}{T} \tag{4.5}$$

In a two-temperature model ($T_{vib} \neq T_{rot}$), the coupling terms are assigned (fully or partly) to either the vibrational term or the rotational term. This assignment is arbitrary. For certain levels, $E_{coupling}$ may be comparable to $\bar{E}_{vib}$ or $\bar{E}_{rot}$. Depending on the chosen assignment, this will lead to different populations for energy levels under nonequilibrium conditions, hence different nonequilibrium spectra. Babou *et al*. [11] investigated the effect of the coupling terms on nonequilibrium partition functions for diatomic molecules. They found that the coupling terms made a quantitative difference for temperatures above 10,000 K.

Following Babou *et al*. [11], we consider two extreme cases. In case 1, we fully assign the coupling terms in Eqn. (4.2) to the vibrational energy:

$$E_{vib} = \bar{E}_{vib} + E_{coupling} \tag{4.6}$$

$$E_{rot} = \bar{E}_{rot} \tag{4.7}$$

$$Q_{rovib}(T_{vib}, T_{rot}) = \sum_{v} \left[\left(\sum_{J} g_v e^{-\frac{\bar{E}_{vib}(v) + E_{coupling}(v,J)}{kT_{vib}}} g_{rot}(J) e^{-\frac{\bar{E}_{rot}(J)}{kT_{rot}}} \right) \right] \tag{4.8}$$

In case 2, we assign the coupling terms to the rotational energy:

$$E_{vib} = \bar{E}_{vib} \tag{4.9}$$

$$E_{rot} = \bar{E}_{rot} + E_{coupling} \tag{4.10}$$

$$Q_{rovib}(T_{vib}, T_{rot}) = \sum_{v} \left[\left(\sum_{J} g_v e^{-\frac{\bar{E}_{vib}(v)}{kT_{vib}}} g_{rot}(J) e^{-\frac{\bar{E}_{rot}(J) + E_{coupling}(v,J)}{kT_{rot}}} \right) \right] \tag{4.11}$$

To use these assignment schemes, we need to determine E_{vib}, E_{rot} and $E_{coupling}$ for each rovibrational level. This contribution is rarely explicitly given: only the total energy of the rovibrational level or the non-diagonalized Hamiltonian of the molecule are known. We thus use the method described in Section 4.2.

4.2 Contribution of the energy modes to the total energy of the rovibrational levels

As for diatomic molecules, certain coupling terms (such as vibrational-rotational coupling) appear as diagonal terms in the Hamiltonian and produce the α_e and β_e terms in the Dunham expansions. Additional coupling terms result from the non-diagonal terms of the Hamiltonian (such as the Fermi coupling, or the l-doubling coupling for the CO_2 molecule). As far as we know, their contribution to the levels' energy is usually not explicitly given.

To determine the contributions of the non-diagonal coupling terms, we use the following procedure: we write $P = (x_{ij})$ the transfer matrix that diagonalizes the Hamiltonian *H*.

$$D = P^{-1}HP \tag{4.1}$$

We define the contribution of energy mode *m* to the energy of level *i* as:

$$C_i^{(m)} = \left(P^{-1}H^{(m)}P\right)_{ii} = \sum_l x_{li} \sum_k h_{lk}^{(m)} x_{ki} \tag{4.2}$$

$C_i^{(m)}$ is the diagonal coefficient of the partial Hamiltonian $H^{(m)}$, corresponding to the energy mode m, transferred into the diagonal basis of H. We can write *H* as a sum of sub-Hamiltonians corresponding to the contributions of all the energy modes *m* as follows:

$$H = \sum_{m \in \{\text{energy modes}\}} H^{(m)} \tag{4.3}$$

The decomposition of the total Hamiltonian into different modes is arbitrary. For example, for the CO_2 molecule, one could split the total Hamiltonian into three vibrational modes, one rotational mode and the coupling mode such as in Eq. (4.4), or into only one vibrational mode, one rotational mode, one sub-Hamiltonian for the Fermi interaction, one for the Coriolis-interaction and one for the other couplings such as in Eq. (4.16):

$$H = \sum_i H_{\text{vib},i} + H_{\text{rot}} + H_{\text{coupling}} \tag{4.4}$$

$$H = H_{\text{vib}} + H_{\text{rot}} + H_{\text{Fermi}} + H_{\text{Coriolis}} + H_{\text{other couplings}} \tag{4.5}$$

Note that $P^{-1}H^{(m)}P$, corresponding to energy modes *m*, are generally not diagonal.

For the CO_2 molecule, using the decomposition proposed in Eq. (4.4), we can write the total energy of level *i* as follows:

$$E_{\text{i}} = \sum_m C_i^{(m)} = \sum_j \tilde{\text{E}}_{\text{vib},j}^{i} + \tilde{\text{E}}_{\text{rot}}^{\text{i}} + \text{E}_{\text{coupling}}^{\text{i}} \tag{4.6}$$

If the levels are not coupled, i.e., H is diagonal[3] and $P = 1$ (identity), therefore $C_i^{(m)} = \left(H^{(m)}\right)_{ii}$.

If the levels *i* inside a polyad are perfectly mixed, i.e., if they cannot be differentiated (for example, the levels of the polyad $p = 1$ of the CO_2 molecule are perfectly mixed through the Fermi interaction), each (perturbed) level receives the same contribution from each energy mode, meaning that the eigenvectors X_i have the same coefficients ($x_j = \frac{1}{N}$ if *j* is inside the polyad, $x_j = 0$ otherwise, and N is the number of levels inside the polyad). For non-perfectly mixed levels, it should then be possible to quantify the character of the levels (in a similar manner as done by [24] to quantify the electronic character of vibronic levels of the N_2 molecule) using a metric based on the coefficients of the eigenvectors for the corresponding polyad[4].

Depending on the number of temperatures used, it is then possible to group the modes following Section 3 and then use the method described in Section 4.1, or to use its generalized form described in Section **Erreur ! Source du renvoi introuvable.** to determine the uncertainties on

[3] There is no inter-level interaction, such as the Fermi interaction.

[4] This will not be discussed further in this paper, but could be the purpose of future work.

the nonequilibrium partition functions. We can thus obtain, for each rovibrational level, a vibrational energy E_{vib}, a rotational energy E_{rot} and the coupling terms energy $E_{coupling}$.

5 Impact of the coupling terms: application to CO_2

5.1 Coupling terms of CO_2

The rovibrational energies of $CO_2(X)$ are computed by using the effective Hamiltonian of Tashkun *et al.* [25]. The effective Hamiltonian is block-diagonalized for polyad numbers $p \leq 40$, and rotational numbers $J \leq 300$. Levels above the dissociation threshold of 44600 cm^{-1} are not considered. A description of the levels within a polyad for CO_2 is given in Appendix A. The total rovibrational energies obtained after diagonalization, E, are found to match the rovibrational energies calculated by Tashkun [26] within the rounding error.

In these calculations, the zero-point-energy (ZPE) is subtracted, with ZPE = 2531.827 cm^{-1}.

Figure 4 shows the contributions of the different energy terms (symmetric stretching, bending and asymmetric stretching vibrational modes, rotational terms and coupling terms: the vibrational coupling terms are noted E_{vib123}, and the vibrational-rotational coupling terms as E_{vibrot}, and Fermi, Coriolis and l-doubling interactions). For the sake of clarity, the contribution of each energy term in Figure 4 is binned over nearby levels with a window of size from 20 to 3,000 cm^{-1}. In our calculations, the exact energy partitioning of every level is used. For energies above 600 cm^{-1} and below 30,000 cm^{-1}, the contribution of the vibrational energy of the bending mode (ν_2) is dominant. Above 30,000 cm^{-1}, rotational energies $\bar{E}_{rot}$ corresponding to high J levels are the main contributors to the total energy.

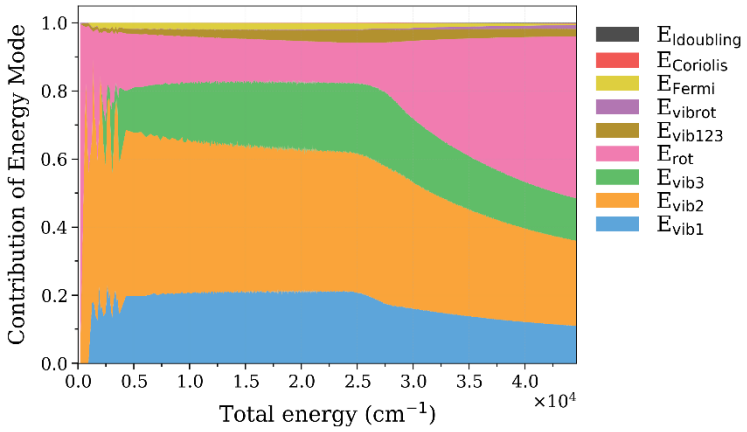

Figure 4 Contribution of each energy term (in absolute value) to the total energy of rovibrational levels (smoothed over adjacent levels).

Figure 5 shows the contributions of the coupling terms to the total rovibrational energy calculated for all rovibrational levels of $^{12}C^{16}O_2(X^1\Sigma_g^+)$, sorted by total energy from 0 cm^{-1} to the dissociation energy, 44,600 cm^{-1}. Each term is shown in absolute values, as some of these terms can be negative. Fermi coupling, E_{Fermi}, and mixed vibrational terms, E_{vib123}, are dominant. For energies above 30,000 cm^{-1}, the rovibrational coupling terms E_{vibrot} of high J levels become important. Nonetheless, the coupling terms represent less than 6% of the total energy of the rovibrational

levels. This confirms that, under equilibrium conditions, the influence of the coupling terms on the partition function is negligible (Eq. (4.5)).

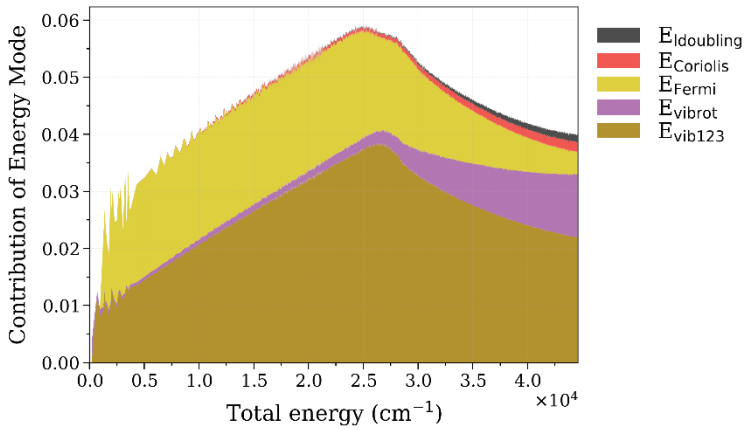

Figure 5 Contribution of the coupling terms (in absolute value) to the total energy of rovibrational levels (smoothed over adjacent levels)

The contribution of the coupling terms is of the same order of magnitude as the contribution of the rotational term or of the asymmetric stretching (ν_3) term: for example, at 25,000 cm^{-1}, $E_{coupling} \approx E_{rot}/2 \approx E_{vib3}/3$. The coupling terms can no longer be neglected compared to the rotational term or the asymmetric stretching term. Their impact on nonequilibrium partition functions will be discussed in Section 5.2.

5.2 Impact of the coupling terms

In Section 3, we examined the influence of the temperature grouping schemes for the CO_2 molecule for the simple case of the UVR model in which the coupling terms are neglected. In this section, we perform the same study, this time incorporating the effect of the coupling terms.

5.2.1 First temperature grouping scheme: all vibrational modes have the same temperature ($T_{vib} = T_{vib1} = T_{vib2} = T_{vib3}$, T_{rot})

For this first temperature grouping scheme, we compare in Figure 6 the partition functions computed with the two assignment schemes presented in Section 4.1 and the partition function computed with the UVR model. The temperatures T_{vib}, T_{rot} range from 300 to 10,000 K.

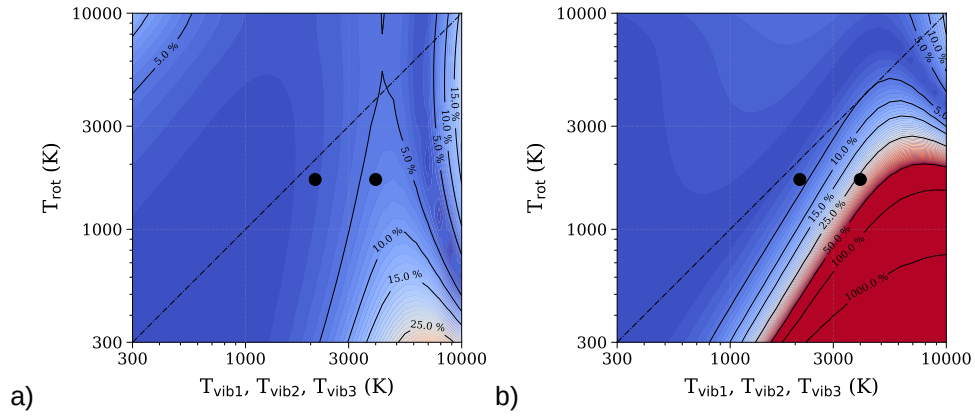

Figure 6 Relative differences between nonequilibrium partition functions calculated using the UVR model and nonequilibrium partition functions computed with the coupling terms assigned to the vibrational energy (a) or

to the rotational energy (b) for $\{T_{vib},T_{rot}\}=\{(T_{vib1}=T_{vib2}=T_{vib3}),T_{rot}\}$. Experiments (circles): expansion-tube [10, 17, 18]**.**

When the coupling terms are assigned to the vibrational energy (Figure 6a), the differences with the UVR model are less than 10% in most of the temperature range considered. This is expected since, with this grouping scheme, the vibrational energy (sum of the energies of the three vibrational modes) is far larger than the coupling term, which can therefore be neglected.

The differences with the UVR model are larger when the coupling terms are assigned to the rotational energy, especially for T_{vib} > 2,000 K and T_{rot}< 2,000 K (Figure 6b). Indeed, as seen in Section 5.1, the coupling terms and the rotational terms are of the same order of magnitude for high rovibrational levels. For example, at 25,000 cm^{-1}, the coupling term is approximately 50% of the rotational term. This means that the coupling terms have a strong impact on the partition functions at low rotational temperatures, when $E_{rot} + E_{coupling} \approx k_B T_{rot}$, and when the vibrational temperature is high enough for high rovibrational levels to be populated, as can be seen in Figure 6.

We now compare in Figure 7 the nonequilibrium rovibrational partition function calculated with the two assignment schemes described in Section 4.1. Near equilibrium ($T_{vib} \approx T_{rot}$), the two schemes give similar results, as expected. This means that the coupling terms can be applied to either the vibrational term or the rotational term without significant changes to the partition functions. When T_{vib} is 2-4 times larger than T_{rot}, however, the partition functions differ drastically. The choice of the assignment scheme strongly impacts the partition functions.

The temperature conditions of the expansion-tube experiments reported in Refs. [10, 17, 18] are represented by the circles on the figures. For these experiments, the partition functions calculated with the two assignment schemes do not differ by more than 25%, and therefore the assignment choice is not crucial for the analysis of these spectra.

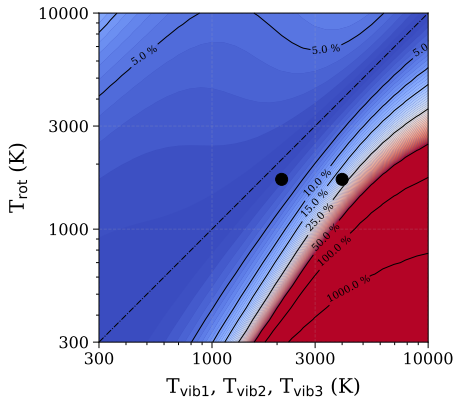

Figure 7 Relative differences between nonequilibrium partition functions calculated with the total coupling terms (inter-vibrational, vibrational-rotational, Fermi, Coriolis, l-doubling) assigned to the vibrational energy or to the rotational energy for $\{T_{vib},T_{rot}\}=\{(T_{vib1},T_{vib2},T_{vib3}),T_{rot}\}$. Experiments (circles): expansion-tube [10, 17, 18]**.**

Using Figure 6 and Figure 7, it is possible to obtain the domains where the UVR model is sufficient (i.e. where the partition functions differ by less than 25%) to accurately describe the CO_2 molecule. These domains are shown in Figure 8. The white area corresponds to the domain where the UVR model is sufficient, meaning that complete models, independently of their assignment schemes, give partition functions within 25% of the UVR partition function. In the grey area, the UVR model and the models with the coupling terms differ, but both coupling assignment schemes give similar results (the partition functions differ by 15 to 25%). In this area, one should take the coupling terms into account but can assign them indifferently to either the vibrational or rotational term.

In the dashed area, all models and assignment schemes give different results, and thus the predicted partition functions and derived quantities (spectra, …) are highly sensitive to the chosen model. Their results are subject to caution. In this case, it is very important to state explicitly which assignment scheme is chosen to analyze the spectra.

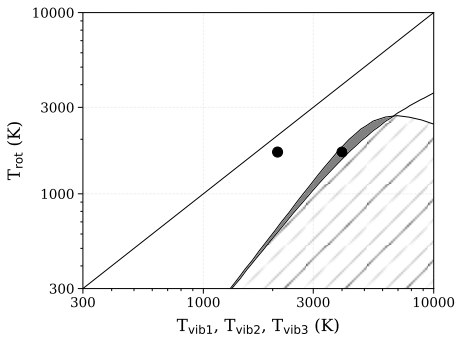

Figure 8 Validity domain of the UVR model, for $\{T_{vib},T_{rot}\}=\{(T_{vib1},T_{vib2},T_{vib3}),T_{rot}\}$. Coupling terms should not be neglected in the grey area but the assignment schemes give similar results. All models and assignment schemes give different results (more than 25% differences) in the dashed area. Experiments: expansion-tube [10, 17, 18] **(circles).**

5.2.2 Second temperature grouping scheme: the asymmetric stretching mode has a different temperature ($T_{vib} = T_{vib3}$, $T_{rot} = T_{vib1} = T_{vib2}$)

For this second temperature grouping scheme, we have $T_{vib} = T_{vib3}$ and $T_{rot} = T_{vib12}$. We compare in Figure 9 the partition functions computed with the two assignment schemes presented in Section 4.1 with the UVR model. The coupling terms are either assigned to the vibrational term (a) or to the rotational term (b).

The temperature conditions of experiments with a CO_2 laser [13] (circles), CO_2 glow discharges [7] (squares) and CO_2 Nanosecond Repetitive Pulse (NRP) discharges [20] (triangles) are shown in the figures.

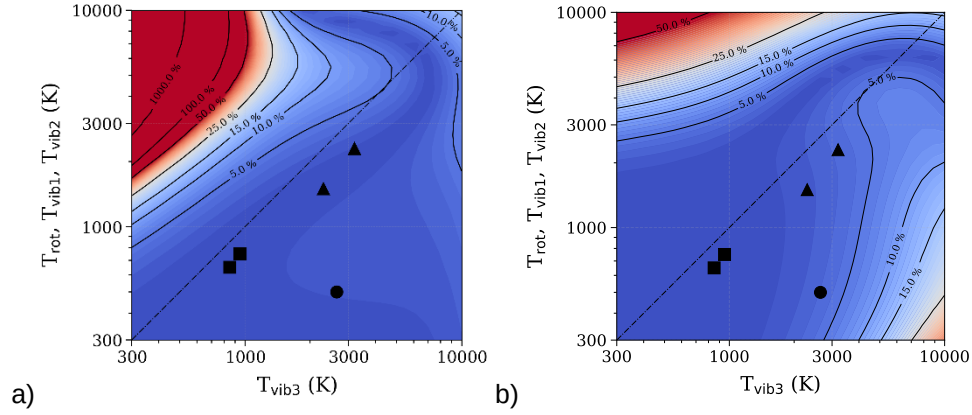

Figure 9 Relative differences between nonequilibrium partition functions calculated using the UVR model and nonequilibrium partition functions computed with the coupling terms assigned to the vibrational energy (a) or to the rotational energy (b) for $\{T_{vib},T_{rot}\}=\{T_{vib3},(T_{rot}=T_{vib1}=T_{vib2})\}$. Experiments: CO_2 laser [13] **(circles), CO_2 glow discharges** [7] **(squares), CO_2 NRP discharges** [20] **(triangles).**

When the coupling terms are assigned to the vibrational energy (Figure 9a), the differences with the UVR model are less than 5% in the temperature range of the experiments. However, the differences are larger when T_{rot} is 2-4 times larger than T_{vib}.

When the coupling terms are assigned to the rotational energy (Figure 9b), the differences with the UVR model are less than 50% in the temperature range considered, and even less than 5% at the temperatures of the experiments shown here. The highest discrepancies are for T_{rot} about 4-10 times larger than T_{vib}.

This is expected since, here, the rotational term (sum of the rotational energy and the energies of the first two vibrational modes) is far larger than the coupling term, which can therefore be neglected in most temperature conditions. For vibrational temperatures above 7,000 K, however, the high energy levels, which are also the levels with the highest coupling energies, contribute more significantly to the partition function, leading to larger discrepancies with the UVR model. Yet, these discrepancies are less than 100% in the temperature range considered, which is far lower than the 1,000% discrepancies that were found when assigning the coupling terms to E_{vib3} (Figure 9a).

We compare in Figure 10 the nonequilibrium rovibrational partition functions for the two assignment schemes presented in Section 4.1. Both assignment schemes yield similar results close to equilibrium, but discrepancies appear for strong nonequilibrium conditions when T_{rot} is 2-4 times larger than T_{vib}. For the experiments reported, the chosen assignment scheme does not change the partition function by more than 5%.

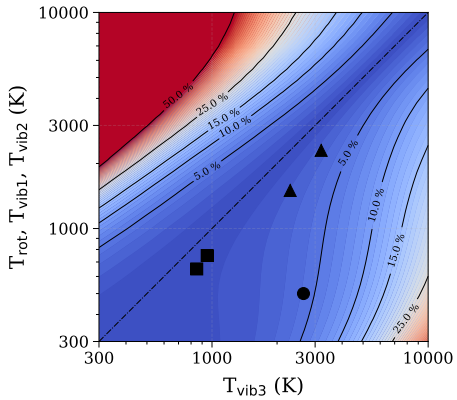

Figure 10 Relative differences between nonequilibrium partition functions calculated with the total coupling terms (inter-vibrational, vibrational-rotational, Fermi, Coriolis, l-doubling) to the vibrational energy or to the rotational energy for $\{T_{vib},T_{rot}\}=\{T_{vib3},(T_{rot},T_{vib1},T_{vib2})\}$. Experiments: CO_2 laser [13] **(circles), CO_2 glow discharges** [7] **(squares), CO_2 NRP discharges** [20] **(triangles).**

Using Figure 9 and Figure 10, we obtain the domains where the UVR model is sufficient to accurately describe the CO_2 molecule as in Section 5.2.1. These domains are shown in Figure 11. The white area corresponds to the domain where the UVR model is valid, i.e., where the different models give partition functions within 25%. In the dashed area, all models and assignment schemes give different results, and thus the predicted partition functions and derived quantities are highly sensitive to the chosen model. The results are subject to caution.

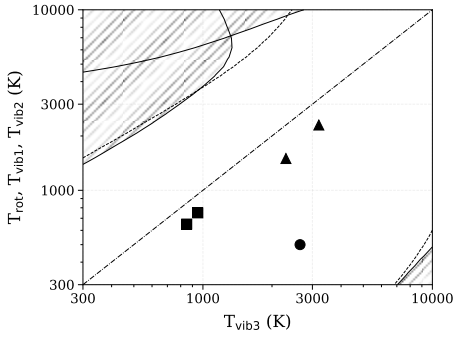

Figure 11 Validity domain of the UVR model, for $\{T_{vib},T_{rot}\}=\{T_{vib3},(T_{rot},T_{vib1},T_{vib2})\}$. In the dashed areas, the various models give partition functions that differ by more than 25%. Experiments: CO_2 laser [13] **(circles), CO_2 glow discharges** [7] **(squares), CO_2 NRP discharges** [20] **(triangles).**

All experimental conditions reported here are within the validity of the UVR model. However, one should be careful at high vibrational temperatures (above 8,000 K) and low rotational temperatures (below 500 K), which is typically the range of nonequilibrium conditions targeted for CO_2 conversion applications. For these conditions, it is necessary to be explicit about the chosen assignment or grouping schemes.

6 Examples for CO_2

To further emphasize the impact of temperature grouping and assignment schemes, we present in Table 1 the numerical values of nonequilibrium partition functions for different temperature conditions. The chosen conditions correspond to 3 experimental cases displayed in the previous figures: first, the CO_2 laser [13] represented by the circle in Figure 11; second, the CO_2 shock [10] represented by a circle in Figure 8; and finally, the CO_2 glow discharges [7] represented by squares in Figure 11.

Table 1 Nonequilibrium partition functions $Q_{rovib}e$ for three different temperature conditions, using the two temperature groupings and the presented assignment schemes.

	First temperature grouping T_{rot} ; $T_{vib} = T_{vib1} = T_{vib2} = T_{vib3}$	Second temperature grouping $T_{rot} = T_{vib1} = T_{vib2}$; $T_{vib} = T_{vib3}$
Case 1	T_{rot} = 491 K ; T_{vib} = 2 641 K	
UVR Model	11 946	824.8
Couplings with E_{rot}	28 0356	866.6
Couplings with E_{vib}	12 850	832.0
Case 2	T_{rot} = 1700 K ; T_{vib} = 4000 K	
UVR Model	142,990	20,143
Couplings with E_{rot}	191,136	21,972
Couplings with E_{vib}	158,675	20,857
Case 3	T_{rot} = 650 K ; T_{vib} = 850 K	
UVR Model	1402	1025
Couplings with E_{rot}	1450	1046
Couplings with E_{vib}	1437	1040.5

The first case has a rotational temperature of 491 K and a vibrational temperature of 2641 K. For the first temperature grouping scheme, this case is within the domain where the coupling terms impact the partition function differently. The partition functions differ by a factor 2.4. The simulated spectra differ significantly, as shown in Figure 12, where the transmittance corresponding to the

first grouping scheme (in red) differs depending on the assignment of the coupling terms. For the second temperature grouping scheme, this case is within the validity domain of the UVR model, as shown in Figure 11. The differences between the partition functions are smaller, and the simulated transmittances (in black) are almost superposed.

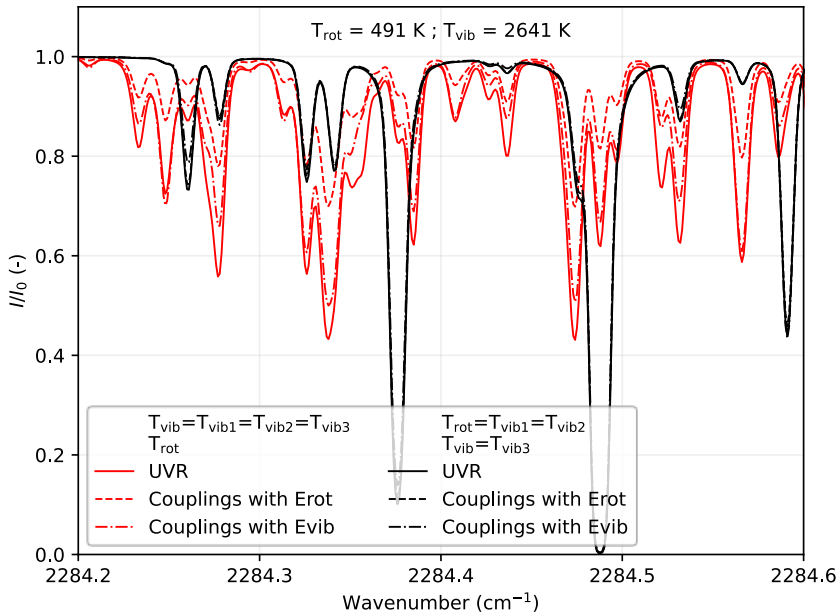

Figure 12 Comparison of transmittances obtained with the two grouping schemes (black and red lines) under the CO_2 laser [13] **experimental conditions, using the UVR model (solid lines), assigning the coupling terms to the rotational energy (dashes) or to the vibrational energy (dash-dots). Computed with a pressure of 20 mbar and a CO_2 mole fraction of 0.0657.**

The second case has a rotational temperature of 1700 K and a vibrational temperature of 4000 K. It is outside the validity domain of the UVR model for the first temperature grouping scheme, and even in the narrow zone where the coupling terms are important but have a similar impact regardless of the assignment scheme. The partition functions differ by approximately 20% if the coupling terms are assigned to E_{rot} or E_{vib}. Figure 13 shows the simulated spectra. In red, the spectra uses the first grouping scheme. The simulated radiances computed with the UVR model or by assigning the coupling terms to E_{rot} differ by up to 35% at 4170 nm. The simulated radiances obtained with the coupling terms differ by 17% approximately. This case is also within the validity domain of the UVR model for the second temperature grouping: the radiances (in black) are within 10% of each other.

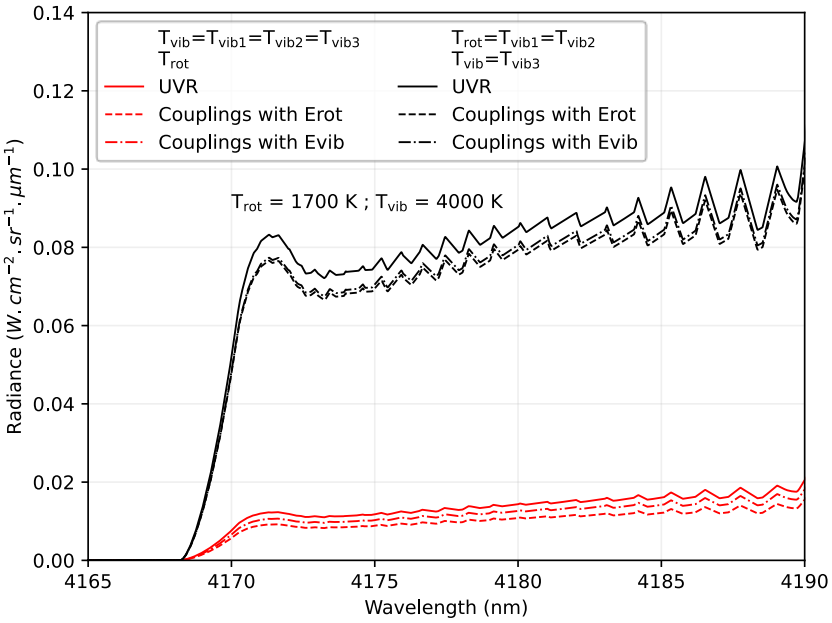

Figure 13 Comparison of radiance using the two grouping schemes (black and red lines) under the CO_2 shock temperatures, using the UVR model (solid lines), assigning the coupling terms to the rotational energy (dashes) or to the vibrational energy (dash-dots). Computed with a pressure of 17 mbar, a CO_2 mole fraction of 0.606 and a slit function of FWHM of 2 nm.

The third case, with a rotational temperature of 650 K and a vibrational temperature of 850 K, is within the domain where the UVR model is sufficient for both temperature groupings. The partition functions have close values for a given temperature grouping scheme (within 3.5%). For the two different temperature grouping schemes, the nonequilibrium conditions induce differences between the partition functions and thus the simulated spectra shown in Figure 14. We observe that the red and black lines are not perfectly superposed: this illustrates the differences between the temperature grouping schemes. However, all three red lines (resp. black lines) are superposed as expected.

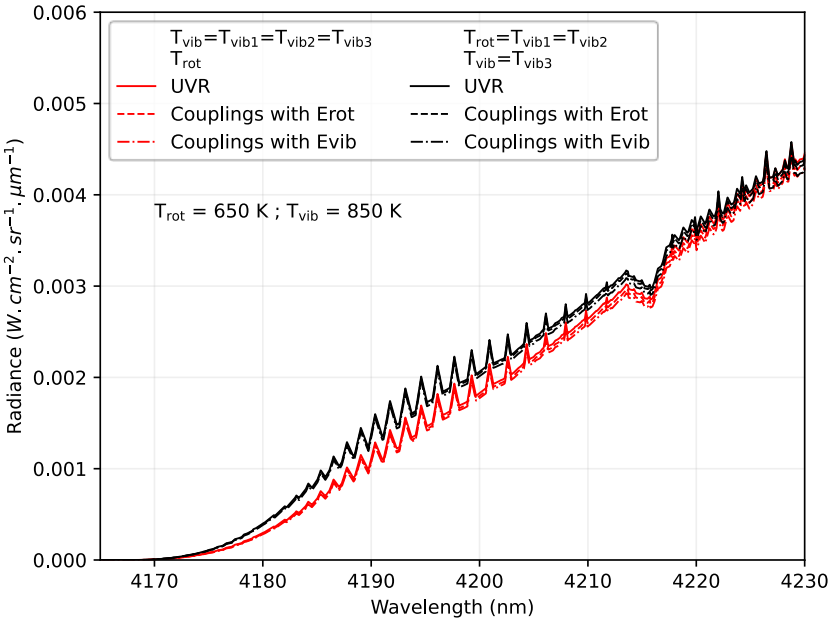

Figure 14 Comparison of radiance using the two grouping schemes (black and red lines) under the CO_2 glow discharge experimental conditions, using the UVR model (solid lines), assigning the coupling terms to the rotational energy (dashes) or to the vibrational energy (dash-dots). Computed with a pressure of 6.7 mbar, a CO_2 mole fraction of 0.0657 and a slit function of FWHM of 2 nm.

These examples highlight the importance of the choice of the temperature grouping for nonequilibrium conditions and of the assignment schemes since they can lead to significant differences in simulated spectra and thus impact the analysis of experimental data.

7 Conclusions

Two-temperature models are often used to characterize nonequilibrium plasmas. They are obtained by lumping the temperatures of the energy modes into two groups: usually, a vibrational temperature and a rotational temperature. In the case of CO_2, for example, the three vibrational modes are sometimes lumped together, and in this case the plasma is described by a two-temperature model, (T_{rot} , T_{vib}), with $T_{vib} = T_{vib1} = T_{vib2} = T_{vib3}$. For plasma discharges, however, several experiments and numerical simulations indicate that a more representative two-temperature grouping scheme may be $T_{rot} = T_{vib1} = T_{vib2}$, and $T_{vib} = T_{vib3}$.

We have shown that the choice of the temperature grouping scheme has a very strong impact on the nonequilibrium partition functions of CO_2. This is the main message of this article. Nonequilibrium partition functions determine the population of internal energy levels, and therefore the emission and absorption spectra. The analysis of experimental spectra is thus very sensitive to the choice of the temperature grouping scheme.

Furthermore, the coupling terms between the various energy modes of the Hamiltonian, and the way to assign them, can also affect the nonequilibrium partition functions. To assess the impact of these coupling terms on two-temperature partition functions, we proceeded in two steps. First, we proposed a method to extract the rotational, vibrational, and coupling energy terms in the diagonal basis of the molecule's Hamiltonian. We applied the method to the CO_2 molecule and showed that although the coupling terms do not represent more than 6% of the total rovibrational energy of the levels, they can be comparable with the rotational or the vibrational energy of the levels.

Second, we compared nonequilibrium partition functions of CO_2 up to 10,000 K with the coupling schemes assigned either to the rotational energy term, or to the vibrational energy term. We then derived zones of confidence where these choices have a limited impact, or where they lead to important differences. We showed that for high vibrational and low rotational temperatures, the coupling assignment strongly affects the partition functions. Furthermore, we compared the results with the simpler UVR model, which neglects all coupling terms. We showed that the UVR model is sufficient over large domains of nonequilibrium conditions, but these domains are extremely dependent on the temperature grouping chosen.

This work can be generalized to other molecules. It is possible to reduce the number of degrees of freedom from n to $p + m$ (with $p \geq 1, m \geq 0$) with physical hypotheses (e.g., assuming a Boltzmann distribution of the levels at a temperature T reduces the number of free parameters from $n = \#\,\text{of levels}$ to $p = 1, m = 0$). When $m \geq 1$, one can quantify the impact of grouping these m degrees of freedom to the p others by comparing extreme cases. Having a direct impact on the absorption and emission spectra, we use nonequilibrium partition functions as a metric to quantify the impact of the different grouping cases on the populations of the rovibrational levels.

In summary, the temperature grouping scheme has a very strong effect on nonequilibrium partition functions of CO_2. The coupling term assignment scheme has a much weaker impact than

the temperature grouping scheme. Unless T_{rot} is low and T_{vib} is high, the nonequilibrium partition functions calculated with the UVR model are generally sufficient. But again, attention must be paid to the choice of the grouping scheme, and based on our analysis of the literature, it is recommended for CO_2 to use a two-temperature model with $T_{rot} = T_{vib1} = T_{vib2}$, and $T_{vib} = T_{vib3}$.

We recommend that all analyses of experimental spectra explicitly indicate the choice of temperature and coupling terms assignment schemes.

References

[1] J. Annaloro, "Elaboration of collisional-radiative models applied to atmospheric entry into the Earth and Mars atmospheres," Ph.D. Thesis, Université de Rouen, 2013.

[2] T. Kozák and A. Bogaerts, "Splitting of CO2 by vibrational excitation in non-equilibrium plasmas: A reaction kinetics model," *Plasma Sources Sci. Technol.*, vol. 23, no. 4, 2014, doi: 10.1088/0963-0252/23/4/045004.

[3] J. F. Vargas, B. Lopez, and M. Lino Da Silva, "High Temperature Applications Of New Vibrationally Specific Kinetics and Radiation Models For CO2," in *AIAA Scitech 2020 Forum*, Jan. 2020, no. January, pp. 1–17, doi: 10.2514/6.2020-1937.

[4] M. Capitelli, G. Colonna, G. D'Ammando, K. Hassouni, A. Laricchiuta, and L. D. Pietanza, "Coupling of Plasma Chemistry, Vibrational Kinetics, Collisional-Radiative Models and Electron Energy Distribution Function Under Non-Equilibrium Conditions," *Plasma Process. Polym.*, vol. 14, no. 1–2, 2017, doi: 10.1002/ppap.201600109.

[5] S. Heijkers, L. M. Martini, G. Dilecce, P. Tosi, and A. Bogaerts, "Nanosecond Pulsed Discharge for CO2 Conversion: Kinetic Modeling to Elucidate the Chemistry and Improve the Performance," *J. Phys. Chem. C*, vol. 123, no. 19, pp. 12104–12116, 2019, doi: 10.1021/acs.jpcc.9b01543.

[6] C. Park, J. T. Howe, R. L. Jaffe, and G. V. Candler, "Review of chemical-kinetic problems of future NASA missions. II - Mars entries," *J. Thermophys. Heat Transf.*, vol. 8, no. 1, pp. 9–23, Jan. 1994, doi: 10.2514/3.496.

[7] B. L. M. Klarenaar, R. Engeln, D. C. M. van den Bekerom, M. C. M. van de Sanden, A. S. Morillo-Candas, and O. Guaitella, "Time evolution of vibrational temperatures in a CO 2 glow discharge measured with infrared absorption spectroscopy," *Plasma Sources Sci. Technol.*, vol. 26, no. 11, p. 115008, Oct. 2017, doi: 10.1088/1361-6595/aa902e.

[8] E. Pannier and C. O. Laux, "RADIS: A nonequilibrium line-by-line radiative code for CO2 and HITRAN-like database species," *J. Quant. Spectrosc. Radiat. Transf.*, vol. 222–223, pp. 12–25, Jan. 2019, doi: 10.1016/j.jqsrt.2018.09.027.

[9] G. Palmer and B. A. Cruden, "Experimental Validation of CO2 Radiation Simulations," *43rd AIAA Thermophys. Conf.*, no. June, pp. 1–15, 2012, doi: 10.2514/6.2012-3188.

[10] H. Takayanagi, A. Lemal, S. Nomura, and K. Fujita, "Measurements of Carbon Dioxide Nonequilibrium Infrared Radiation in Shocked and Expanded Flows," *J. Thermophys. Heat Transf.*, vol. 32, no. 2, pp. 483–494, Apr. 2018, doi: 10.2514/1.T5200.

[11] Y. Babou, P. Rivière, M. Y. Perrin, and A. Soufiani, "High-temperature and nonequilibrium partition function and thermodynamic data of diatomic molecules," *Int. J. Thermophys.*, vol. 30, no. 2, pp. 416–438, 2009, doi: 10.1007/s10765-007-0288-6.

[12] R. R. Gamache *et al.*, "Partition sums for non-local thermodynamic equilibrium conditions for nine molecules of importance in planetary atmospheres," *Icarus*, p. 114947, 2022, doi: 10.1016/j.icarus.2022.114947.

[13] C. Dang, J. Reid, and B. K. Garside, "Detailed vibrational population distributions in a CO2 laser discharge as measured with a tunable diode laser," *Appl. Phys. B Photophysics Laser Chem.*, vol. 27, no. 3, pp. 145–151, 1982, doi: 10.1007/BF00694640.

[14] R. K. Koopmann and A. R. Saunders, "Nonequilibrium population distributions for vibrational energy levels of CO2 in CO-O2 flames at reduced pressure," *J. Quant.*

Spectrosc. Radiat. Transf., vol. 10, no. 5, pp. 403–421, May 1970, doi: 10.1016/0022-4073(70)90106-8.

[15] A. Lombardi, N. Faginas-Lago, L. Pacifici, and A. Costantini, "Modeling of Energy Transfer From Vibrationally Excited CO 2 Molecules: Cross Sections and Probabilities for Kinetic Modeling of Atmospheres, Flows, and Plasmas," *J. Phys. Chem. A*, vol. 117, no. 45, pp. 11430–11440, 2013, doi: 10.1021/jp408522m.

[16] E. E. Whiting, C. Park, Y. Liu, J. O. Arnold, and J. A. Paterson, "NEQAIR96, Nonequilibrium and Equilibrium Radiative Transport and Spectra Program: User's Manual," 1996.

[17] K. Fujita and T. Abe, "SPRADIAN, Structured Package for Radiation Analysis:Theory and Application," Institute of Space and Astronautical Science Report no. 669, September 1997.

[18] E. Pannier and C. O. Laux, "Analysis of the JAXA Nonequilibrium Infrared Emission Spectra for Mars Entry Conditions," *J. Thermophys. Heat Transf.*, vol. 33, no. 4, pp. 1127–1131, 2019, doi: 10.2514/1.T5646.

[19] U. Dubuet, S. Nomura, S. Matsuyama, A. Lemal, H. Takayanagi, and K. Fujita, "Simulations of CO2-CO Infrared Radiation Measurements in Shock and Expansion-Tubes," *J. Thermophys. Heat Transf.*, 2020, doi: 10.2514/1.T5853.

[20] E. Pannier, "Conversion of Carbon Dioxide with Nanosecond Pulsed Discharges," Ph.D. Thesis, Université Paris-Saclay, 2019.

[21] S. A. Tashkun and V. I. Perevalov, "CDSD-4000: High-resolution, high-temperature carbon dioxide spectroscopic databank," *J. Quant. Spectrosc. Radiat. Transf.*, vol. 112, no. 9, pp. 1403–1410, Jun. 2011, doi: 10.1016/j.jqsrt.2011.03.005.

[22] L. Pierrot, "Chemical kinetics and vibrationally-specific collisional-radiative models for nonequilibrium nitrogen plasmas," ESA Post-Doctoral Fellowship Report, July, 1999.

[23] Y. Liu and M. Vinokur, "Equilibrium gas flow computations. I - Accurate and efficient calculation of equilibrium gas properties," *24th Thermophysics Conference*, Jun. 1989, doi: 10.2514/6.1989-1736.

[24] D. Stahel, M. Leoni, and K. Dressler, "Nonadiabatic representations of the 1Σu+ and 1Πu states of the N2 molecule," *J. Chem. Phys.*, vol. 79, no. 6, pp. 2541–2558, 1983, doi: 10.1063/1.446166.

[25] S. A. Tashkun, V. I. Perevalov, J. L. Teffo, L. S. Rothman, and V. G. Tyuterev, "Global Fitting of 12C16O2 Vibrational-Rotational Line Positions Using the Effective Hamiltonian Approach," *J. Quant. Spectrosc. Radiat. Transf.*, vol. 60, no. 5, pp. 785–801, Nov. 1998, doi: 10.1016/S0022-4073(98)00082-X.

[26] S. A. Tashkun, "C12O16O16 energy levels (private communication)." .

[27] L. S. Rothman *et al.*, "the Hitran Molecular Spectroscopic Database and Hawks (Hitran Atmospheric Workstation): 1996 Edition," *J. Quant. Spectrosc. Radiat. Transf.*, vol. 60, no. 5, pp. 665–710, 1998, doi: 10.1016/S0022-4073(98)00078-8.

[28] S. A. Tashkun, V. I. Perevalov, J. L. Teffo, A. D. Bykov, and N. N. Lavrentieva, "CDSD-1000, the high-temperature carbon dioxide spectroscopic databank," *J. Quant. Spectrosc. Radiat. Transf.*, vol. 82, no. 1–4, pp. 165–196, 2003, doi: 10.1016/S0022-4073(03)00152-3.

[29] S. C. Wang, "On the asymmetrical top in quantum mechanics," *Phys. Rev.*, vol. 34, no. 2, pp. 243–252, 1929, doi: 10.1103/PhysRev.34.243.

[30] H. M. Pickett, "The fitting and prediction of vibration-rotation spectra with spin interactions," *J. Mol. Spectrosc.*, vol. 148, no. 2, pp. 371–377, 1991, doi: 10.1016/0022-2852(91)90393-O.

[31] J. M. Brown *et al.*, "The Labeling of Parity Doublet Levels in Linear Molecules," vol. 55, pp. 500–503, 1975.

[32] G. Herzberg, *Molecular Spectra and Molecular Structure. II. Infrared and Raman Spectra of Polyatomic Molecules*. 1964.

[33] M. E. Kellman, “Approximate constants of motion for vibrational spectra of many-oscillator systems with multiple enharmonic resonances,” *J. Chem. Phys.*, vol. 93, no. 9, pp. 6630–6635, 1990, doi: 10.1063/1.458930.

Appendix: CO_2 nomenclature

We describe the different CO_2 rovibrational level nomenclatures found in literature, recalling the interaction selection rules and the alternation of rotational levels that characterize CO_2. Figure 15 shows the first rovibrational levels of ground state $^{12}C^{16}O_2$, for $p \leq 3$ and the $J \leq 4$. For the sake of clarity, rotational energies are shown on an expanded scale.

A. Conventions

The usual (Herzberg) notation uses the 5 quantum numbers $v_1v_2^{l_2}v_3[J]$, where v_1, v_2, v_3 are the vibrational quantum numbers of the symmetric mode ν_1, bending mode ν_2, and asymmetric mode ν_3; when the bending mode ν_2 is excited, rotation around the molecular axis can occur and the l_2 quantum number is introduced to quantify the projection of the resultant vibrational angular momentum. l_2 can take the values v_2, $v_2 – 2$, … 1 or 0. J is the rotational quantum number ($J \geq l_2$).

The unperturbed symmetric mode has approximately twice the energy (ν_1 = 1333.93 cm^{-1}) of the unperturbed bending mode (ν_2 = 667.47 cm^{-1}), and so the Fermi interaction is particularly strong between levels that share the same $2v_1+v_2$ number and the same angular momentum l_2. For every value of v_3, the 10^0v_3 and 12^0v_3 levels interact and form a Fermi dyad; the 20^0v_3, 12^0v_3 and 04^0v_3 levels form a Fermi triad, and generally speaking the levels with the same $2v_1+v_2$ value form a Fermi interacting polyad. The energies of Fermi polyads levels are shifted, and the usual nomenclature fails to describe them unambiguously.

To remove this ambiguity, HITRAN [27] introduced the *spectroscopic* notation with 6 quantum numbers $v_1v_2^{l_2}v_3r[J]$: levels are first grouped in generalized polyads (which may contains several Fermi polyads), defined as all levels that share the same polyad number $p=2v_1+v_2+3v_3$. Within a polyad p, a Fermi polyad is defined for all combinations of l_2 and v_3. It can be shown that a Fermi polyad (function of p, v_3 and l_2) contains $(p-l_2-3v_3)/2+1$ interacting states if l_2 has the same parity as $p-3v_3$, and none otherwise. Within each Fermi polyad, the values of v_1 and v_2 are arbitrarily fixed, and the sixth quantum number r is introduced to label the levels unambiguously. The rules chosen to set v_1, v_2 and r are as follow:

- $2v_1=p-3v_3-l_2$
- $v_2=l_2$
- $1 \leq r \leq v_1+1$ where levels are ranked by decreasing energy

The HITRAN labelling scheme is based on the proper assignment of the l_2 quantum number. For high rotational numbers, when additional interaction terms become significant (l-doubling and Coriolis coupling), the l_2 number cannot be defined unambiguously and the HITRAN notation itself becomes ambiguous [25]: the CDSD-1000 [28] and CDSD-4000 [21] database introduced the *generalized* denomination (p, c, J, N), where $p=2v_1+v_2+3v_3$ is the polyad number, c is the Wang symmetry type, J is the rotational quantum number, and N is a ranking number for levels of a (p, c, J) block sorted by increasing energy. The Wang symmetry results from the choice of a proper basis to further reduce the Hamiltonian in two non-interacting blocks (*e* and *f*). More details on the choice of the Wang basis can be found in [18–20].

On Figure 15, the rovibrational levels are given in usual notation (black). The corresponding HITRAN notation (green) and CDSD notation (red) are also given for rovibrational levels with $p \leq 2$. As explained above, because of the Fermi coupling shift (blue), the labelling of the levels in a Fermi polyad (for instance, $10^00 – 02^00$, or $11^00 – 03^00$) become ambiguous. They have been arbitrary labelled here but could as well have been inverted ($02^00 – 10^00$, and $03^00 – 11^00$, respectively). The HITRAN and CDSD notations, however, remain unambiguous by construction.

B. Symmetry types

Vibrational levels of CO_2 have different symmetry types Σ, Π, Δ, etc., which correspond to values of the orbital angular momentum l_2 = 0, 1, 2, etc. respectively. Symmetry *type* is also called *species* in Herzberg [32]. For $l_2 > 0$, the vibrational levels are doublets, with their degeneracy removed by l-doubling for high rotational numbers.

For instance, in the usual convention, the polyad p=2 corresponds to the vibrational levels $v_1v_2v_3$=100, 020, with degeneracies 1 and 3. The second harmonic of the bending mode, 020, has two sublevels 02^20 and 02^00 of Δ and Σ symmetry, respectively. 02^20 is a doublet (l>0), 02^00 is a singlet, hence the g=3 degeneracy for 020. Eventually, the p=2 polyad contains four vibrational states: 10^00, $02^20(\Delta^+)$, $02^20(\Delta^-)$, 02^00. Doublets appear on Figure 15 although for the CO_2 626 isotope, only one level exist within every doublet for spin-symmetry reasons detailed in the next paragraph.

C. Parity and symmetry

Figure 15 shows the g/u symmetry of vibrational levels, which alternates with the vibrational number for the bending and asymmetric modes; and the +/- parity of rotational level, which alternates with J. The rotational symmetry (s/a) of the rotational level is inferred from both the vibrational symmetry and the rotational parity: for a *gerade* (g) vibrational level, +/- rotational levels have s/a symmetry, for *ungerade* (u) vibrational levels +/- rotational levels have a/s symmetry.

The statistical weight of the symmetric and asymmetric rotational levels is determined by the spins of pairs of identical nuclei. For the symmetric isotopes of CO_2, such as the main $^{12}C^{16}O_2$ isotope, the ratio of symmetric over asymmetric statistical weights is 1:0, *i.e.*, asymmetric rotational levels are missing. In Figure 15, missing rotational levels appear with dashed lines. In RADIS, the spin-dependency of the statistical weight is included in the state-independent degeneracy g_i. Values for the HITRAN molecules can be found in Ref [32].

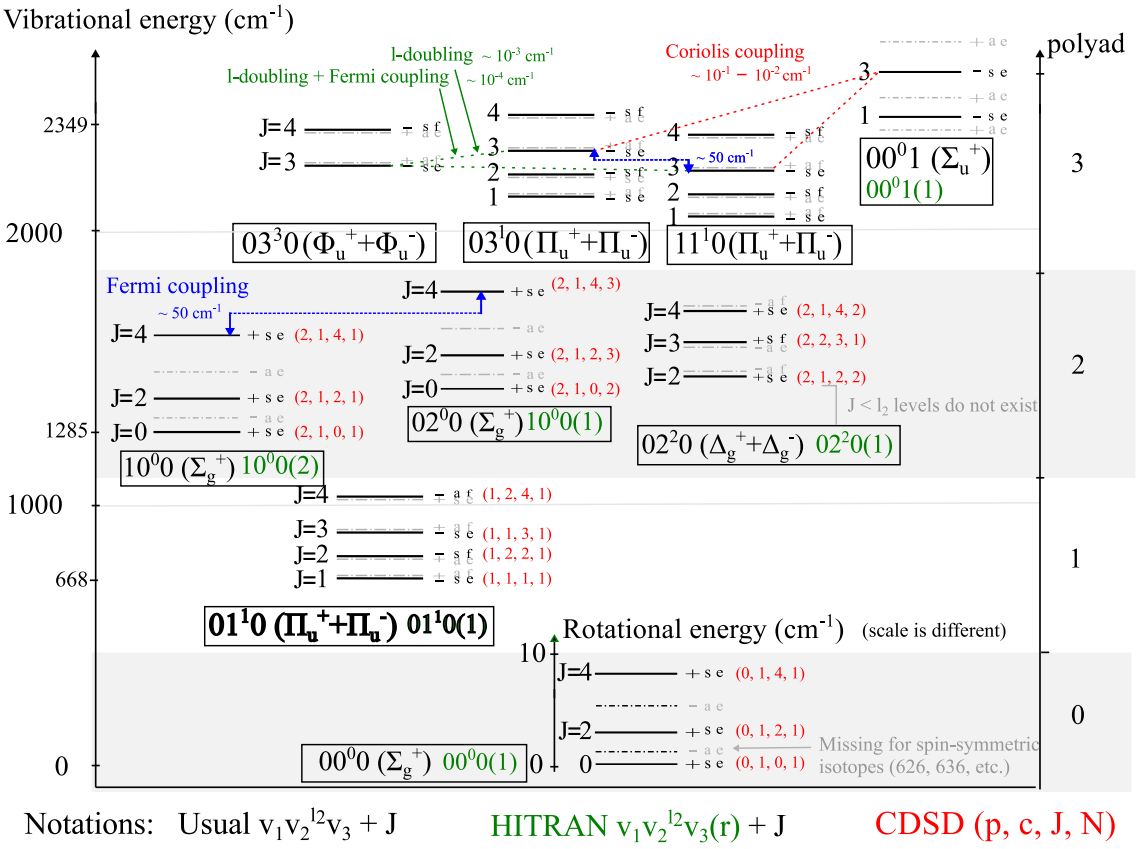

Figure 15 First rovibrational levels of ground-state CO_2, up to polyad number p=3, described in the usual notation with +/- parity, a/s symmetry, and e-f parity (black). Corresponding labels in HITRAN (green) and CDSD (red) notation are given. Solid lines: existing states. Fermi, Coriolis, l-doubling interaction terms are shown for p=2, J=4 and p=3, J=3 levels. Dotted lines: missing states in spin-symmetric isotopes (as $^{12}C^{16}O_2$, $^{13}C^{6}O_2$). Rotational levels are shown on a different scale from vibrational levels. Refer to text for more details.

D. Perturbation selection rules

Rovibrational energy levels can interact if they share the same J number, and the same rovibrational parity (+, or -) [32]. The interaction can be without rotation (Fermi coupling), or induced by rotation (Coriolis coupling). Fermi coupling terms are usually stronger (typically 50 cm^{-1} for CO_2, compared to about 1 cm^{-1} for Coriolis coupling), but they require, on top of the previously mentioned selection rules, that both levels share the same symmetry types. In CO_2, Fermi coupling only happens between the ν_1 vibration states, all of which are Σ states, and the Σ states of the v_2 vibration mode. Figure 15 summarizes the different interaction terms for the p=2, J=4 and p=3, J=3 levels.

In the usual notation, the rotational states are also given an e/f parity, which has been introduced for linear polyatomic molecules in Ref. [31] to extend the notation used in diatomic molecules. It is used to rewrite perturbation selection rules as follows [12,31]: levels can interact (↔) if they have the same rotational number (J ↔ J), the same parity (e ↔ e, f ↔ f), and, for rotationless perturbations (Fermi coupling), the same orbital momentum: $l_2 \leftrightarrow l_2$. In the CDSD notation, the e/f parity corresponds to the Wang number c used. The e, f parity appears on Figure 15 for all levels of low-lying polyads p≤3.